Fusion reaction of halo nuclei: A real-time wave-packet method for three-body tunneling dynamics

Takashi Nakatsukasa*, Makoto Ito†**, Kazuhiro Yabana* and Manabu Ueda‡

*Institute for Physics and Center for Computational Sciences, University of Tsukuba, Tsukuba 305-8571, Japan
†Institute for Physics, University of Tsukuba, Tsukuba 305-8571, Japan
**RIKEN, Hirosawa 2-1, Wako, Saitama 351-0198, Japan
‡Akita National College of Technology, Akita 011-8511, Japan

Abstract. We investigate fusion cross section of a nucleus with a valence neutron, using the time-dependent wave-packet method. For a stable projectile, in which the valence neutron is tightly bound ($\varepsilon_n < -3$ MeV), the neutron could enhance the fusion probability when the matching condition of orbital energies are satisfied. In contrast, for a halo nucleus, in which the binding energy of the neutron is very small ($\varepsilon_n > -1$ MeV), the fusion probability is hindered by the presence of the weakly bound neutron.

INTRODUCTION

The fusion cross section around the Coulomb barrier energy has been investigated for a long time [1]. The cross sections sometimes significantly differ from nucleus to nucleus depending on properties of nuclear internal structures. Intrinsic excitations of a projectile and a target during the collision affect the fusion cross section. For weakly bound nuclei, excitations to the continuum, that is breakup as well as transfer process, are expected to play a very important role. Since such low-energy reaction cannot be described properly by (semi-)classical theories, the full quantum-mechanical reaction theory is necessary. We have developed a method using the time-dependent wave-packet (TDWP) for description of the fully quantum reaction dynamics of a few-body systems [2, 3, 4, 5, 6]. An advantage of the TDWP method is given by an intuitive visualization of dynamics of the quantum reaction. In practical aspects, the time evolution of the wave packet does not require complicated scattering boundary conditions.

There have been contradictory predictions on the fusion cross section of a halo nucleus at sub-barrier energies, even among calculations using similar models. We have been studying the fusion probability of halo ^{11}Be on ^{208}Pb [3, 4, 5]. The total fusion cross section (CF+ICF) of ^{11}Be was predicted to be smaller than that of ^{10}Be around the Coulomb barrier energies. Namely, the presence of a halo neutron leads to a suppression of the fusion probability. On the contrary, the coupled discretized continuum channels (CDCC) calculations, employing a three-body model very similar to ours, show a strong enhancement of the total fusion cross section at sub-barrier energies for ^{11}Be on ^{208}Pb

[7, 8]. We have identified that this discrepancy comes from different truncation for relative angular momentum, ℓ, between the neutron and the ^{10}Be core [3, 6]. Our calculation includes the partial waves up to $\ell = 70\,\hbar$, while the CDCC does up to $\ell = 4\,\hbar$ at most. Actually, when we truncate the partial waves in the same way as the CDCC calculations do ($\ell \leq 4\,\hbar$), we also produce the strong sub-barrier fusion enhancement. However, this enhancement completely disappears as we include higher partial waves in the calculation.

Importance of the higher partial waves seems to suggest that the neutron breakup and transfer from ^{11}Be take place in an oriented manner. In fact, we have found that the halo neutron is emitted toward the target, then some part of the neutron wave packet is caught by the target potential ("transfer") and the rest escapes to the free space ("breakup"). This leads to a simple spectator picture of the halo nucleus: Since the halo neutron is very weakly bound, it easily escapes from the binding of the projectile and hardly changes its velocity, while the ^{10}Be core is decelerated by the Coulomb potential from the target. This leads to loss of the effective colliding energy of ^{10}Be because the escaped neutron carries about $1/11$ of the original projectile energy. This accounts for obtained reduction of the fusion cross section.

In this article, we compare the fusion process of neutron halo nuclei with that of stable nuclei. Different dynamical effects of a valence neutron are discussed and we further elucidate a spectator picture of fusion dynamics of halo nuclei.

TDWP METHOD AND APPLICATIONS

We describe a projectile (P) as a two-body bound system of a core nucleus (denoted as C) and a valence neutron (n). In this work, the neutron is assumed to occupy a single-particle orbital of $\ell = 0$ (s-wave). The projectile collides with a target (T) which is assumed to be in the ground state all the time. The time-dependent Schrödinger equation for the three-body model is given by

$$i\hbar\frac{\partial}{\partial t}\Psi(\boldsymbol{R},\boldsymbol{r},t) = \left\{-\frac{\hbar^2}{2\mu}\nabla^2_{\boldsymbol{R}} - \frac{\hbar^2}{2m}\nabla^2_{\boldsymbol{r}} + V_{\mathrm{nC}}(r) + V_{\mathrm{CT}}(R_{\mathrm{CT}}) + V_{\mathrm{nT}}(r_{\mathrm{nT}})\right\}\Psi(\boldsymbol{R},\boldsymbol{r},t), \quad (1)$$

where the relative n-C coordinate is denoted as $\boldsymbol{r}$ and the relative P-T coordinate as $\boldsymbol{R}$. The reduced masses for the n-C and P-T motions are m and μ, respectively. The real potential, $V_{\mathrm{nC}}(r)$, produces a projectile and controls binding energy of the neutron in the projectile. The neutron-target potential, $V_{\mathrm{nT}}(r_{\mathrm{nT}})$, is also real. This potential controls the orbital energies in the target and affects properties of transfer reaction. The core-target potential, $V_{\mathrm{CT}}(R_{\mathrm{CT}})$, consists of nuclear and Coulomb potentials. The nuclear part contains an imaginary part inside the Coulomb barrier between the core and the target. When the wave function has its amplitude inside the barrier, a part of the flux will be lost. This absorption describes the fusion of the core and target nuclei. We define the fusion cross section in terms of the loss of flux, which is almost equivalent to the definition using the incoming boundary condition inside the barrier. Since we do not calculate the wave function of the fused system in this framework, we cannot distinguish the complete

fusion (CF) process from the incomplete one (ICF). Thus, the fusion cross section we show in this article represents the total fusion cross section (CF+ICF).

The wave function has six variables, $\boldsymbol{R}$ and $\boldsymbol{r}$. We transform the equation in the laboratory frame to the one in the body-fixed frame. Then, the variables are three Euler angles (α,β,γ), an angle θ between $\boldsymbol{R}$ and $\boldsymbol{r}$, and two radial variables, R and r. The wave function is expressed in a form

$$\Psi^{JM}(R,r,\alpha,\beta,\gamma,\theta;t)=\sum_{\Omega}^{J}\sum_{\ell}^{\ell_{\max}}\frac{u^{J}_{\Omega\ell}(R,r;t)}{Rr}G^{JM}_{\Omega\ell}(\alpha,\beta,\gamma,\theta), \tag{2}$$

where the angle function $G^{JM}_{\Omega\ell}$ is expressed by the D-function, $D^{J}_{\Omega M}(\boldsymbol{\omega})$, and the associated Legendre polynomials, $P^{\Omega}_{\ell}(\cos\theta)$ [9, 10]. The wave-packet method is suited for the body-fixed representation because it can take an advantage of the sparsity of the Coriolis couplings.

In order to prepare an initial wave packet for the three-body system, first, the wave function for projectile is constructed as an eigenstate of the core-neutron Hamiltonian, $\phi_0(r)$. Then, it is multiplied by a localized Gaussian boosted toward the collision, $u(R,r,t=0)=\phi_0(r)\exp(-(R-R_0)^2/2\lambda-iKR)$. The parameters, λ and K, are chosen so as to cover an energy range of interest. A single time evolution of the wave packet contains all the information for this range of incident energy. We perform calculations of the energy projection for the wave packets before and after the collision, to obtain the rate of flux loss as a function of incident energy.

The radial coordinates, R and r, are discretized in mesh of $0.2\sim1$ fm. The discrete variable representation is utilized in evaluation of the differentiation. The time evolution is achieved by the fourth-order Taylor expansion. Details are found in our recent papers[3, 4, 5, 6].

Case I: Stable projectile

First, we investigate fusion reaction of a stable projectile. For the projectile in which the valence neutron is rather tightly bound, the fusion cross section is normally identical to that without the valence neutron. However, when the condition of energy matching is satisfied, which means that energies of the neutron orbital in the projectile and target are degenerate, we may observe a substantial enhancement of sub-barrier fusion cross section. This can be seen in Fig. 1. The TDWP calculations are performed with a fictitious ^{11}Be nucleus, in which the valence neutron has a binding energy of 3.5 MeV at the 2s orbital. The depth of $V_{\rm nC}(r)$ is increased to produce this situation.

We vary the depth of the neutron-target potential, $V_{\rm nT}$, and compare the fusion probabilities. The results show that the fusion probability is correlated with the neutron transfer probability and sensitive to $V_{\rm nT}$. When the orbital energies in projectile and target are equal, the fusion probability is enhanced at energies below the barrier while it is suppressed above the barrier (dotted line in Fig. 1). This is caused by large neutron transfer from the projectile to the target. Time evolution of the neutron density distribution during the collision process is shown in Fig. 2. Quantities, $\rho(r,\theta;t)=\int dR|\Psi^{00}(R,r,\theta;t)|^2$,

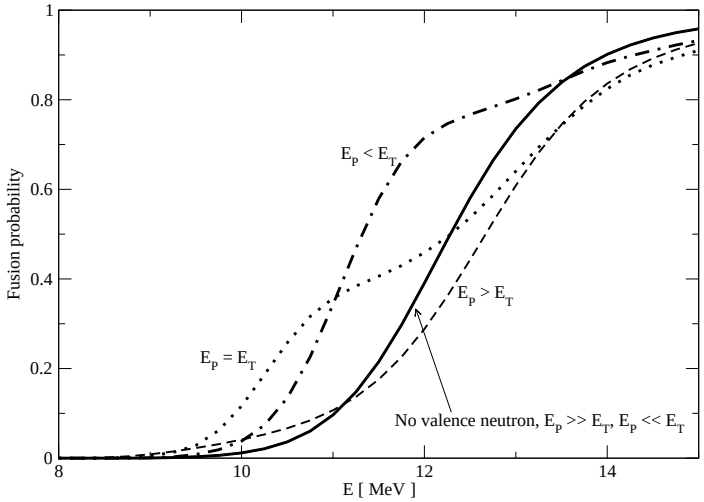

FIGURE 1. Fusion probability ($J = 0$) as a function of incident energy for a tightly bound "^{11}Be" nucleus ($\varepsilon_n = -3.5$ MeV) on ^{40}Ca. Solid line indicates the probability for the projectile without the valence neutron. Dotted, Dashed, and Dash-dotted lines indicate fusion probabilities calculated with different $V_{\rm nT}$ potentials which give orbital energies in the target of -3.5, -5.1, -2.0 MeV, respectively. See text for details.

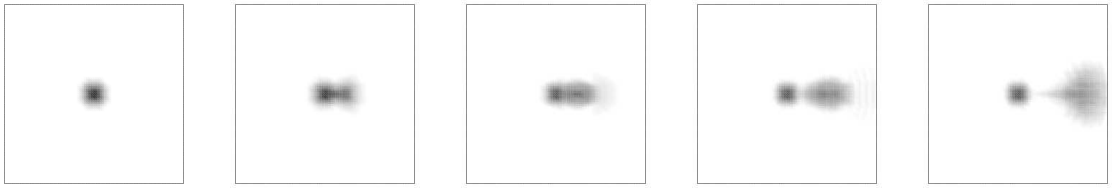

FIGURE 2. Time-dependent density distribution of the valence neutron, $\rho(r,\theta;t)$, corresponding to the dotted line in Fig. 1. The left-end panel is the initial distribution and the right-end shows the final distribution after the collision. The center of each panel, $r = 0$, indicates the position of the core, and the right is the direction for the target, $\theta = 0$. The target nucleus (wave packet) approaches toward the center (the first to second panels), then leaves away to the right (the third to fifth panels).

are plotted for the head-on collision of $J = 0$. Since the direction of the target always corresponds to $\theta = 0$, the target nucleus approaches from the right side of the panel, then returns back to the right. From the second to the fourth panels, we see that the neutron constitutes a kind of molecular orbital extended over both projectile and target. Since the energy matching is good in this case, this results in the large neutron transfer at the final state. The breakup component turns out to be small.

The sub-barrier fusion enhancement is even more pronounced when the $V_{\rm nT}$ becomes slightly shallower than the exact matching case (dash-dotted line in Fig. 1). The opposite effect is observed if the $V_{\rm nT}$ is made slightly deeper (dashed line). This may suggest adiabatic dynamics of the valence neutron. Namely, coupling between orbitals in projectile and target either increase or decrease the kinetic energy of the projectile, according to the relative position of orbital energies [2].

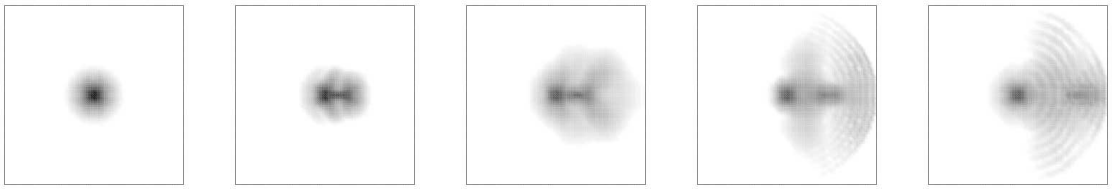

FIGURE 3. Time-dependent density distribution of the halo neutron, for the head-on collision, $J = 0$, of halo ^{11}Be on ^{209}Bi. See caption of Fig. 2.

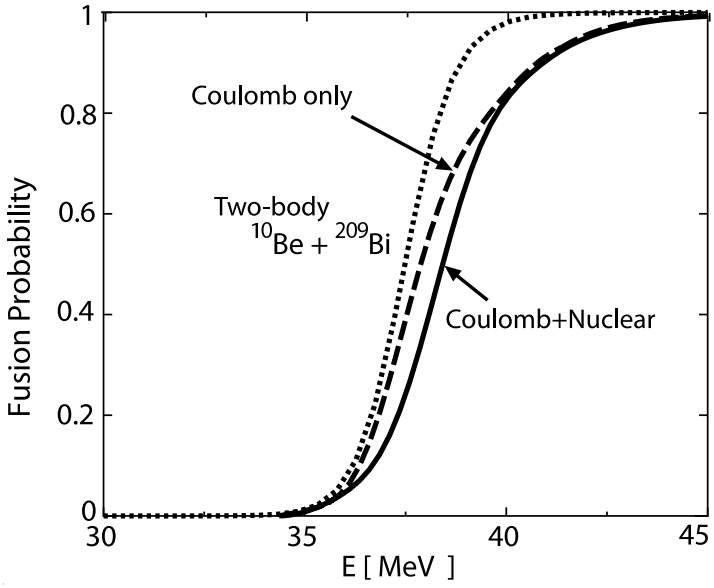

FIGURE 4. Fusion probability ($J = 0$) as a function of incident energy for halo ^{11}Be ($\varepsilon_n = -0.6$ MeV) on ^{209}Bi. Dotted line indicates the probability for the projectile without the valence neutron. Dashed and solid lines indicate fusion probabilities calculated with and without $V_{\rm nT}$ potentials, respectively. See text for details.

Case II: Halo projectile

In the previous section, we have shown that, for the fusion reaction of stable projectiles, the neutron transfer could play a role of "glue" at sub-barrier energies, if the energy matching is good between core and target orbitals. Then, what about halo projectiles? The neutron wave function is well extended out of the core nucleus, producing a large r.m.s. radius. Does this lead to even stronger enhancement of fusion probability? As far as our three-body model is concerned, the answer is "No". The spectator picture of halo neutron, that is given in the introduction of the present article, can give an intuitive understanding of dynamics of halo nuclei.

In Fig. 3, the time evolution of neutron density is shown for a case of good energy matching between core and target orbitals. The neutron energy is set at -0.6 MeV to describe halo ^{11}Be. Comparing this with Fig. 2, we may notice large breakup components of neutron in the halo case. The breakup neutron is expanding in forward directions of

$|\theta| < 90^\circ$. This is consistent with the spectator role of the halo neutron. Since the V_{nT} potential is chosen to satisfy the energy matching between the core and target orbitals, we may identify some transfer components in the panel at the right end. However, in contrast to the case of stable projectiles, the transferred neutron does not play a role of "glue" at all. In Fig. 4, the fusion probability is shown as a function of energy. As is seen in this figure, the neutron-target potential, V_{nT}, changes the fusion probability very little. At all energies, the fusion probability of ^{11}Be is suppressed compared to that of ^{10}Be. This leads to a simple conclusion; The halo neutron leads to a suppression of fusion cross section.

SUMMARY

Effects of a valence neutron on fusion cross section have been studied with the time-dependent wave-packet method in the three-body model. For stable projectiles, the fusion cross section could be enhanced by the presence of the valence neutron, if the orbital energies in the projectile and target are almost equal. However, there is no enhancement for the halo projectile. The fusion cross section is suppressed by the halo neutron, which can be explained by the spectator role of the halo neutron. Comparison with experiments has been done in Ref. [6]. At least, recent measurements indicate no enhancement of fusion cross section for halo nuclei, ^{11}Be on ^{209}Bi [11] and ^{6}He on ^{238}U [12]. Our results are consistent with these data.

ACKNOWLEDGMENTS

This work has been supported by the Grant-in-Aid for Scientific Research in Japan (Nos. 17540231 and 17740160). A part of the numerical calculations have been performed at SIPC, University of Tsukuba, at RCNP, Osaka University, and at YITP, Kyoto University.

REFERENCES

1. M. Dagupta, D. J. Hinde, N. Rowley, and A. M. Stefanini, *Annu. Rev. Nucl. Part. Sci.* **48**, 401–461 (1998).
2. K. Yabana, *Prog. Theor. Phys.* **97**, 437–450 (1997).
3. K. Yabana, M. Ueda, and T. Nakatsukasa, *Nucl. Phys. A* **722**, 261c–266c (2003).
4. T. Nakatsukasa, K. Yabana, M. Ito, M. Kobayashi, and M. Ueda, *Prog. Theor. Phys. Suppl.* **154**, 85–91 (2004).
5. K. Yabana, M. Ito, M. Kobayashi, M. Ueda, and T. Nakatsukasa, *Nucl. Phys. A* **738**, 303–307 (2004).
6. M. Ito, K. Yabana, T. Nakatsukasa, and M. Ueda, Phys. Lett. B in press, URL `http://xxx.lanl.gov/abs/nucl-th/0506073`,
7. K. Hagino, A. Vitturi, C. H. Dasso, and S. M. Lenzi, *Phys. Rev. C* **61**, 037602 (4 pages) (2000).
8. A. Diaz-Torres, and I. J. Thompson, *Phys. Rev. C* **65**, 024606 (6 pages) (2002).
9. R. T. Pack, *J. Chem. Phys.* **60**, 633–639 (1974).
10. B. Imanishi, and W. von Oertzen, *Phys. Rep.* **155**, 29–136 (1987).
11. C. Signorini, et al., *Nucl. Phys. A* **735**, 329–344 (2004).

12. R. Raabe, et al., *Nature* **431**, 823–826 (2004).